On Resonance and Shielding of Printed Traces on a Circuit Board

JEAN-FU KIANG, MEMBER, IEEE

Abstract—**A rigorous formulation in the spectral domain is used to investigate the radiation from unterminated traces printed on a circuit board in the frequency range from 30 MHz to 1 GHz. Both the effect of coupling among adjacent traces on the resonant frequencies, and the shielding effectiveness of metallic coating on the plastic cover are analyzed. It is found that the radiation around resonant frequencies is critical to comply with the FCC specifications, and an appropriate coating can resolve the problem.**

I. Introduction

THE Federal Communications Commission (FCC) regulations for class-B computing devices require that radiated emission at 3 m from the products have to be below a specified limit in the frequency range from 30 MHz to 1 GHz [1]. One way to avoid radiated emission is to route all the signal lines in between two ground planes. However, for more complicated circuit designs, the signal lines are routed not only in between but are also outside of the two ground planes because the number of signal lines exceeds the capacity available between two ground planes. The signal lines outside of the ground planes contribute to the radiation.

The radiation characteristics of microstrip antennas have been widely studied mainly for applications in communications [2]–[5]. However, they are scarcely considered for the printed traces on the circuit boards used in class-B computing devices in the frequency range from 30 MHz to 1 GHz. Understanding radiation properties in this frequency range is necessary to have the circuit board design comply with FCC specifications.

A metallic coating on the plastic cover has been used to shield radiation from computing devices to the neighboring equipments. However, little information is available about its effectiveness. In [6], the shielding effectiveness of a metallic coating is studied. A plane wave of normal incidence is assumed, and the shielding effectiveness is a function of the material properties only. In [7], the radiating sources of high-impedance and low-impedance nature are also considered. However, the results cannot be used to study the radiation from printed traces on the circuit boards in which the structure is more complicated.

In this paper, we try to understand the radiation characteristics of unterminated traces printed on a circuit board. The properties of drivers and loads are not considered here.

Manuscript received November 8, 1989; revised May 14, 1990.

The author was with the Thomas J. Watson Research Center, IBM Corporation, Yorktown Heights, NY 10598. He is now with Bellcore, Red Bank, NJ 07701.

IEEE Log Number 9037878.

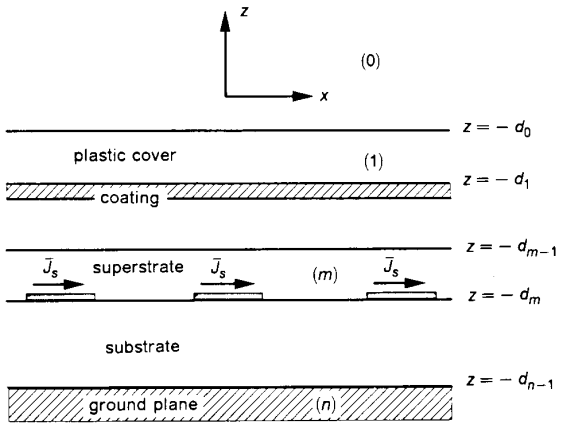

Fig. 1. Geometrical configuration of printed traces embedded in a multilayered medium.

Instead, we focus on the occurrence of resonances and the shielding effectiveness of coating.

First, we use a spectral domain approach to formulate the problem of printed traces radiating in a stratified medium. The substrate, plastic cover, and metallic coating are all considered to be layers of the stratified medium. A set of coupled integral equations are obtained by imposing the boundary condition. The surface currents on the traces are represented by a set of rooftop basis functions [8]. The Galerkin's method [9] is then used to solve the integral equation for the current distribution. The radiation field can be obtained by using the stationary phase integration method [10]. The effects of geometrical parameters and material properties are also investigated.

II. Mathematical Formulation

The geometrical configuration of printed traces on a circuit board with cover and coating is shown in Fig. 1, where there are N parallel traces embedded in layer (m) of a general stratified medium consisting of $(n+1)$ layers. The stratification is perpendicular to the z axis, and the conductivity, dielectric constant, and thickness of layer (m) are σ_m, ϵ_m, and h_m, respectively. All the traces are assumed to be along the y direction, and the width and length of the nth trace are w_n and L_n, respectively.

The electric field in layer (l) can be represented as [9]–[11]

$$\bar{E}(\bar{r}) = i\omega\mu_0 \iint dS' \bar{\bar{G}}_{lm}(\bar{r}, \bar{r}') \cdot \bar{J}_s(\bar{r}') \qquad (1)$$

where we assume that the currents exist on the surface of

traces, and the dyadic Green's function $\bar{\bar{G}}_{lm}(\bar{r}, \bar{r}')$ can be represented in the spectral domain as

$$\bar{\bar{G}}_{lm}(\bar{r}, \bar{r}') = \frac{i}{8\pi^2} \iint_{-\infty}^{\infty} d\bar{k}_s e^{i\bar{k}_s \cdot (\bar{r}_s - \bar{r}'_s)} \bar{\bar{g}}_{lm}(\bar{k}_s, z, z') \tag{2}$$

where

$$\bar{k}_s = \hat{x}k_x + \hat{y}k_y$$
$$\bar{r}_s = \hat{x}x + \hat{y}y$$
$$\bar{r}'_s = \hat{x}x' + \hat{y}y'$$

and $\bar{\bar{g}}_{lm}(\bar{k}_s, z, z')$ is the Fourier transform of $\bar{\bar{G}}_{lm}(\bar{r}, \bar{r}')$ with respect to $\bar{r}_s$. The explicit forms of $\bar{\bar{g}}_{lm}(\bar{k}_s, z, z')$ are shown in the Appendix. In this paper, the time dependence of $e^{i\omega t}$ is assumed.

For our problem, only transversal currents $\bar{J}_s$, having no z component exist. Substituting (2) into (1), the electric field in layer (l) is thus given by

$$\bar{E}(\bar{r}) = -\frac{\omega\mu_0}{2} \iint_{-\infty}^{\infty} d\bar{k}_s e^{i\bar{k}_s \cdot \bar{r}_s} \bar{\bar{g}}_{lm}(\bar{k}_s, z, z') \cdot \bar{K}_s(\bar{k}_s) \tag{3}$$

where $\bar{K}_s(\bar{k}_s)$ is the Fourier transform of the surface current $\bar{J}_s(\bar{r}_s)$ on the trace surfaces, i.e.

$$\bar{K}_s(\bar{k}_s) = \frac{1}{4\pi^2} \iint_{-\infty}^{\infty} d\bar{r}_s e^{-i\bar{k}_s \cdot \bar{r}_s} \bar{J}_s(\bar{r}_s). \tag{4}$$

The electric field in (1) satisfies all the boundary conditions at the interfaces between adjacent layers. We impose the remaining boundary condition that the total tangential electric field vanishes on the surface of the traces, assuming that the traces are made of perfect conductor. Thus, we obtain the following coupled integral equations:

$$\hat{n} \times \left[\bar{E}^c(\bar{r}) - \bar{E}^i(\bar{r})\right] = 0, \quad \bar{r} \text{ on } A_n, \quad 1 \le n \le N \tag{5}$$

where $\bar{E}^c(\bar{r})$ is the electric field generated by the surface current on the traces, A_n is the surface of the nth trace with normal vector $\hat{n}$, and $\bar{E}^i(\bar{r})$ is the electric field generated by the driving sources that are assumed to be delta gap voltage sources. The electric field generated at the jth delta gap is

$$\bar{E}^i_j(\bar{r}) = \begin{cases} -\hat{y}v_j\,\delta(y - y_{0j})\,\delta(z - z_{0j}), \\ \qquad |x - x_{0j}| \le w_{p(j)}/2 \\ 0, \qquad \text{elsewhere} \end{cases} \tag{6}$$

where v_j is the amplitude of the jth delta gap voltage source with center coordinate (x_{0j}, y_{0j}, z_{0j}), and $p(j)$ is the index of the trace where the jth delta gap is located.

III. Numerical Solution

In this paper, we consider straight traces with open termination on general circuit boards, where the length of traces is much longer than the width. Hence, the transversal surface current is much smaller than the longitudinal one and can be neglected. To solve (5), we first choose a set of rooftop basis functions [8] to represent the surface current as

$$\bar{J}_s^{(n)}(\bar{r}_s) = \hat{y} \sum_{j=1}^{N_n} \alpha_{nj} Q(x - x_n, w_n) P(y - y_{nj}, l_n), \quad 1 \le n \le N \tag{7}$$

where $\bar{J}_s^{(n)}(\bar{r}_s)$ is the surface current on the nth trace, α_{nj}'s are the unknowns to be solved, (x_n, y_{nj}) are the center coordinates of the jth basis function on the nth trace, N_n is the number of basis functions on the nth trace, and $l_n = 2L_n/(N_n + 1)$. The explicit forms of $Q(x, a)$ and $P(y, b)$ are

$$Q(x, a) = \begin{cases} 1, & |x| \le a/2 \\ 0, & \text{elsewhere} \end{cases} \tag{8}$$

and

$$P(y, b) = \begin{cases} (2/b)(y + b/2), & -b/2 \le y \le 0 \\ -(2/b)(y - b/2), & 0 \le y \le b/2 \\ 0, & \text{elsewhere.} \end{cases} \tag{9}$$

The Fourier transform of $Q(x, a)$ and $P(y, b)$ are

$$\tilde{Q}(k_x, a) = \frac{\sin(k_x a/2)}{\pi k_x} \tag{10}$$

and

$$\tilde{P}(k_y, b) = \frac{4\sin^2(k_y b/4)}{\pi b k_y^2}. \tag{11}$$

Next, we take the Fourier transform of (7), substitute it into (3) by making use of (4), and then impose the boundary condition (5). Galerkin's method is then applied to solve the coupled integral equations to obtain the following matrix equation:

$$-\frac{\omega\mu_0}{2} \sum_{n=1}^{N} \sum_{j=1}^{N_n} \alpha_{nj} \iint_{-\infty}^{\infty} d\bar{k}_s e^{i\bar{k}_s \cdot (\bar{r}_{rk} - \bar{r}_{nj})} g_{yy}(\bar{k}_s, z_{rm}, z_{nm}) \tilde{Q}(k_x, w_r) \tilde{Q}(k_x, w_n) \cdot \tilde{P}(k_y, l_r) \tilde{P}(k_y, l_n) = \sum_{i=1}^{N_e} \frac{v_i w_r}{4\pi^2} \delta_{rp(i)} \delta_{kq(i)}, \quad 1 \le r \le N, 1 \le k \le N_r \tag{12}$$

where $\bar{r}_{rk} = \hat{x}x_r + \hat{y}y_{rk}$, $\bar{r}_{nj} = \hat{x}x_n + \hat{y}y_{nj}$, and N_e is the number of delta gaps, and $g_{yy}(\bar{k}_s, z_{rm}, z_{nm})$ is the yy component of $\bar{\bar{g}}(\bar{k}_s, z_{rm}, z_{nm})$. $p(i)$ and $q(i)$ are the indices of the trace and the basis on which the ith delta gap is located. The even/odd parity of the Fourier transform of the basis functions and the Green's function with respect to $k_x = 0$ and $k_y = 0$ is utilized to reduce CPU time in computing the double integral in (12).

IV. Radiation Fields

The radiation electric field in region (0) can be calculated by using (1) directly. To reduce the computation time, we

use the stationary phase integration approach [10] to obtain

$$\bar{E}_f(\bar{r}) = \frac{2\pi k_0 \cos\theta}{ir} e^{ik_0 r} \cdot \left[\hat{x}F_x(\theta,\phi) + \hat{y}F_y(\theta,\phi) + \hat{z}F_z(\theta,\phi)\right] \quad (13)$$

where k_0 is the propagation constant in region (0), and (r,θ,ϕ) are the spherical coordinates of the observation point with respect to the origin. The following expressions are obtained when the traces are not directly exposed to region (0):

$$F_x(\theta,\phi) = \sum_{n=1}^{N} K_{ny}(\bar{k}_s) \cdot \left\{ -\frac{k_x k_y k_{0z} X^{\mathrm{TM}}_{\cup 0}\left(e^{-ik_{mz}z_{nm}} - R^{\mathrm{TM}}_{\cap m} e^{ik_{mz}(2h_m + z_{nm})}\right)}{2\omega\epsilon_m k_s^2 \left(1 - R^{\mathrm{TM}}_{\cup m} R^{\mathrm{TM}}_{\cap m} e^{2ik_{mz}h_m}\right)} + \frac{k_x k_y \omega\mu_0 X^{\mathrm{TE}}_{\cup 0}\left(e^{-ik_{mz}z_{nm}} + R^{\mathrm{TE}}_{\cap m} e^{ik_{mz}(2h_m + z_{nm})}\right)}{2k_{mz} k_s^2 \left(1 - R^{\mathrm{TE}}_{\cup m} R^{\mathrm{TE}}_{\cap m} e^{2ik_{mz}h_m}\right)} \right\} \quad (14)$$

$$F_y(\theta,\phi) = \sum_{n=1}^{N} K_{ny}(\bar{k}_s) \cdot \left\{ -\frac{k_y^2 k_{0z} X^{\mathrm{TM}}_{\cup 0}\left(e^{-ik_{mz}z_{nm}} - R^{\mathrm{TM}}_{\cap m} e^{ik_{mz}(2h_m + z_{nm})}\right)}{2\omega\epsilon_m k_n^2 \left(1 - R^{\mathrm{TM}}_{\cup m} R^{\mathrm{TM}}_{\cap m} e^{2ik_{mz}h_m}\right)} - \frac{k_x^2 \omega\mu_0 X^{\mathrm{TE}}_{\cup 0}\left(e^{-ik_{mz}z_{nm}} + R^{\mathrm{TE}}_{\cap m} e^{ik_{mz}(2h_m + z_{nm})}\right)}{2k_{mz} k_s^2 \left(1 - R^{\mathrm{TE}}_{\cup m} R^{\mathrm{TE}}_{\cap m} e^{2ik_{mz}h_m}\right)} \right\} \quad (15)$$

$$F_z(\theta,\phi) = \sum_{n=1}^{N} K_{ny}(\bar{k}_s) \cdot \frac{k_y X^{\mathrm{TM}}_{\cup 0}\left(e^{-ik_{mz}z_{nm}} - R^{\mathrm{TM}}_{\cap m} e^{ik_{mz}(2h_m + z_{nm})}\right)}{2\omega\epsilon_m \left(1 - R^{\mathrm{TM}}_{\cup m} R^{\mathrm{TM}}_{\cap m} e^{2ik_{mz}h_m}\right)} \quad (16)$$

where $k_s = |\bar{k}_s|$, $z_{nm} = z_n + d_{m-1}$, $k_x = k_0 \sin\theta\cos\phi$, $k_y = k_0 \sin\theta \sin\phi$, and $k_{0z} = k_0 \cos\theta$.

In case the traces are directly exposed to region (0), the following expressions are used:

$$F_x(\theta,\phi) = \sum_{n=1}^{N} K_{ny}(\bar{k}_s) \cdot \left\{ -\frac{k_x k_y k_{0z}}{2\omega\epsilon_0 k_s^2}\left(1 - R^{\mathrm{TM}}_{\cap 0}\right) + \frac{k_x k_y \omega\mu_0}{2k_{0z} k_s^2}\left(1 + R^{\mathrm{TE}}_{\cap 0}\right) \right\} \quad (17)$$

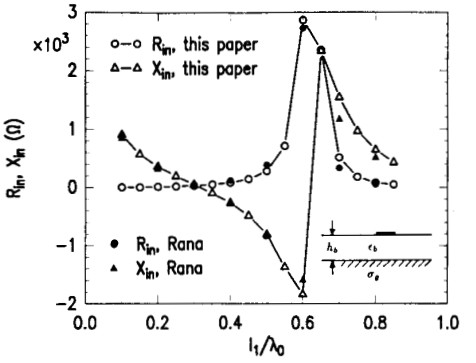

Fig. 2. Input impedance of a printed antenna, where $w_1 = \pi \times 10^{-4}\lambda_0$, $N_1 = 9$, $p(1) = 1$, $q(1) = 5$, $\epsilon_b = 3.25\epsilon_0$, $\sigma_g = 5.92 \times 10^7$ S/m, $h_b = 0.1016\lambda_0$.

$$F_y(\theta,\phi) = \sum_{n=1}^{N} K_{ny}(\bar{k}_s) \cdot \left\{ -\frac{k_y^2 k_{0z}}{2\omega\epsilon_0 k_s^2}\left(1 - R^{\mathrm{TM}}_{\cap 0}\right) - \frac{k_x^2 \omega\mu_0}{2k_{0z} k_s^2}\left(1 + R^{\mathrm{TE}}_{\cap 0}\right) \right\} \quad (18)$$

$$F_z(\theta,\phi) = \sum_{n=1}^{N} K_{ny}(\bar{k}_s) \frac{k_y}{2\omega\epsilon_0}\left(1 - R^{\mathrm{TM}}_{\cap 0}\right). \quad (19)$$

V. Numerical Results and Discussions

First, we present the input impedance of a center-driven microstrip antenna printed on a substrate with ground plane, as is shown in Fig. 2. The results in [4] are also shown for comparison. Since we use the time dependence of $e^{-i\omega t}$, positive (negative) reactance means capacitive (inductive) reactance. Here, N_i is the number of basis functions used on the ith trace, and $p(i)$ and $q(i)$ are the indices of the trace and the basis function where the ith delta gap is located. The width of the trace is chosen to be the same as the circumference of the cylindrical dipole antenna in [4].

In Fig. 3(a), we present the magnitude of current moment on a trace as a function of frequency. The current moment on trace n is defined as

$$\bar{m}_n = \iint_{A_n} dx\,dy\,\bar{J}_s^{(n)}(\bar{r}_s) \quad (20)$$

where $\bar{J}_s^{(n)}(\bar{r}_s)$ is the current distribution on trace n. In general, the magnitude increases with frequency. At the resonant frequency, the magnitude increases by more than two orders. The width of the trace is much shorter than the length but is comparable to the substrate thickness. The frequencies where resonances occur are basically determined by the trace length.

The magnitude of current moment is chosen mainly to demonstrate the occurrence of resonances. When the trace length is smaller than half a wavelength, the radiation field increases as the magnitude of current moment increases. Here, the wavelength means the wavelength of the dominant mode along the direction of the printed trace as if the trace is of infinite length.

The input resistance and reactance of the same structure

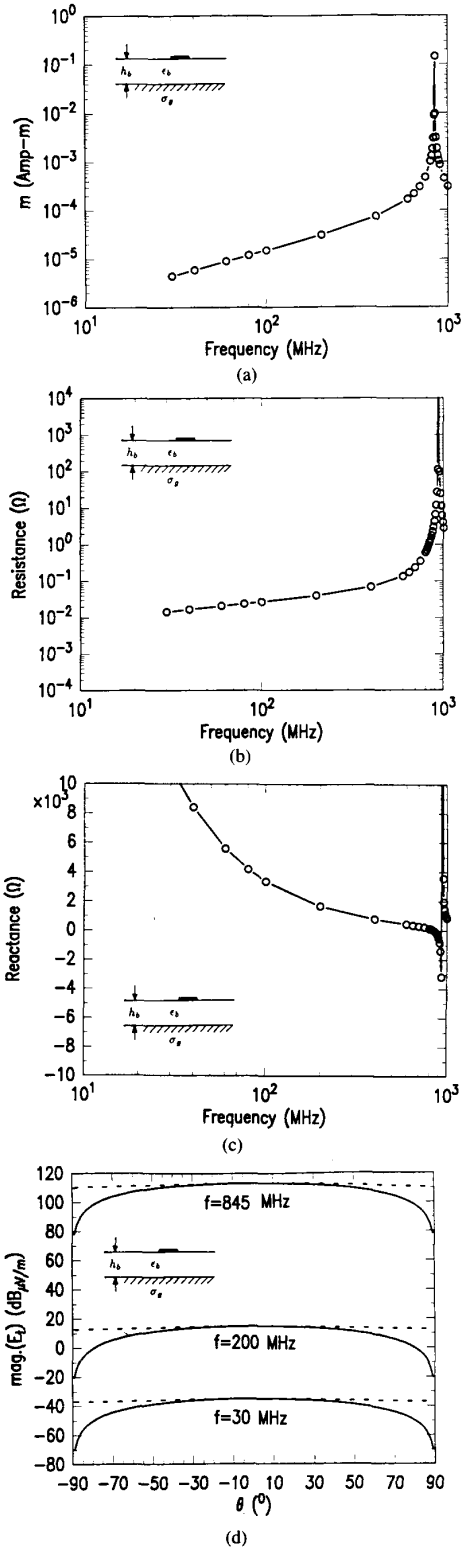

Fig. 3. Characteristics of a printed trace, where $L_1 = 10$ cm, $w_1 = 150$ μm, $N_1 = 9$, $v_1 = 1$ V, $p(1) = 1$, $q(1) = 1$, $\epsilon_b = 4.7\epsilon_0$, $\sigma_g = 5.92 \times 10^7$ S/m, $H_b = 500$ μm: (a) magnitude of current moment; (b) input resistance; (c) input resistance; (d) magnitude of tangential electric field calculated at 3 m, —— E_ϕ at $\phi = 0°$, - - - - E_θ at $\phi = 90°$.

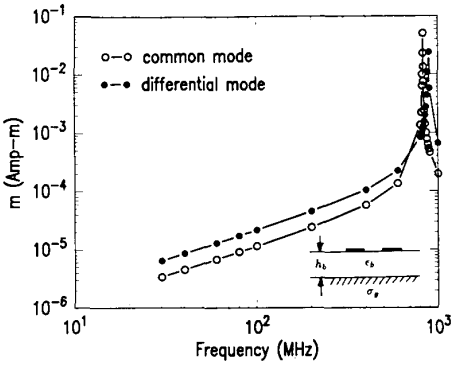

Fig. 4. Magnitude of current moment on two coupled traces, where $L_1 = L_2 = 10$ cm, $w_1 = w_2 = 150$ μm, $c_1 = (-150, 0)$ μm, $c_2 = (150, 0)$ μm, $N_1 = N_2 = 9$, $v_1 = 1$ V, $v_2 = \pm 1$ V, $p(1) = 1$, $p(2) = 2$, $q(1) = q(2) = 1$, $\epsilon_b = 4.7\epsilon_0$, $\sigma_g = 5.92 \times 10^7$ S/m, $h_b = 500$ μm.

are shown in Fig. 3(b) and (c), respectively. It is found that the input resistance is negligibly small below the resonant frequency and possesses a peak around 940 MHz. The input reactance is much larger than the input resistance below the resonant frequency, and reduces to zero around the resonant frequency. The input reactance switches from a large negative number to a large positive number around 940 MHz, which is typical of a thin antenna. This implies that the trace behaves like a capacitor at low frequencies with little radiation and behaves like an antenna around resonant frequency.

The radiation field patterns on the E plane (YZ plane) and the H plane (XZ plane) are shown in Fig. 3(d). It is observed that at low frequencies, the strength of radiation is below the FCC specification, but around the resonant frequency, the radiation strength is far beyond the specification.

Next, we study the coupling effect between two identical traces that are parallel to each other. In Fig. 4, the magnitude of current moment for both the common and differential modes are displayed as a function of frequency. Here, c_i is the transversal center coordinate of the ith trace. The common (differential) mode is defined as the mode driven by two sources that are in (out of) phase.

The resonant frequency of the common mode is different from that of the differential mode. It has been found that the radiation from a common mode is much stronger than that from a differential mode [12], especially in the low frequency range. However, the situation is reversed near the resonant frequency of the differential mode.

In Fig. 5, we present the magnitude of current moment on three coupled traces. In Fig. 5(a) and (b), the driving source is located on the second trace, and two even resonant modes are excited near 810 and 890 MHz. The magnitude of current moment on the third trace is the same as that on the first trace due to symmetry, hence, it is not displayed. In Fig. 5(c), the driving source is located on the first trace, and another resonant frequency of the odd mode is observed around 880 MHz.

The dips at 770 MHz on the first trace and at 820 MHz on the second trace are due to the definition of current moment. At these two frequencies, the current has an oscillatory distribution and gives a smaller quantity after integration

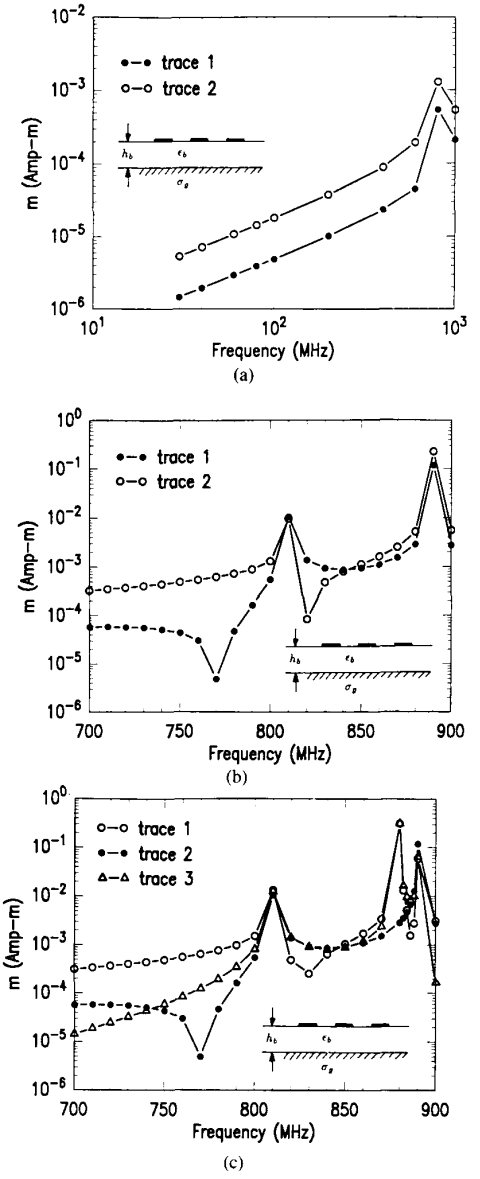

Fig. 5. Magnitude of current moment on three coupled traces, where $L_1 = L_2 = L_3 = 10$ cm, $w_1 = w_2 = w_3 = 150$ μm, $c_1 = (-300, 0)$ μm, $c_2 = (0, 0)$, $c_3 = (300, 0)$ μm, $N_1 = N_2 = N_3 = 9$; $\epsilon_b = 4.7\epsilon_0$, $\sigma_g = 5.92 \times 10^7$ S/m, $h_b = 500$ μm: (a), (b) $v_1 = 1$ V, $p(1) = 2$, $q(1) = 1$; (c) $v_1 = 1$ V, $p(1) = 1$, $q(1) = 1$.

through (20).

Next, we calculate the magnitude of current moment on four coupled traces by applying an even and an odd arrangement of driving sources, respectively. In both cases, resonances occur between 700 and 900 MHz. Hence, we present only the results in this frequency range.

In Fig. 6(a), two even resonant modes are observed around 800 and 890 MHz. In Fig. 6(b), two odd resonant modes are observed around 870 and 890 MHz. The resonant frequencies of all these four modes are different from that of a single trace driven by the same delta gap voltage source.

Next, the effects of plastic cover and metallic coating are

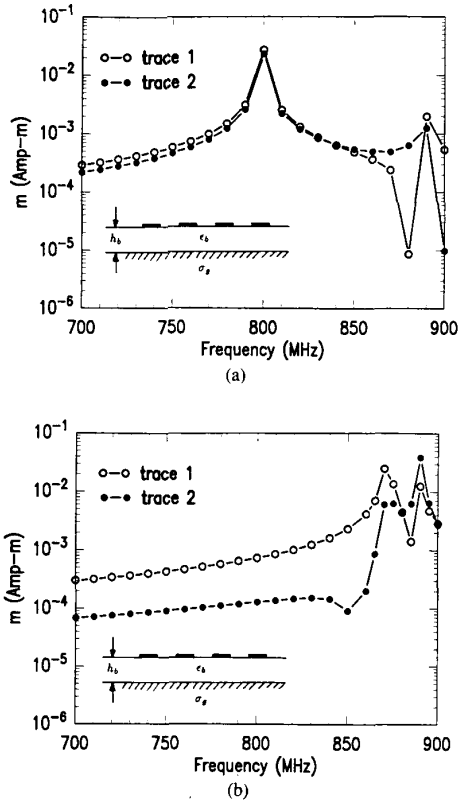

Fig. 6. Magnitude of current moment on four coupled traces, where $L_1 = L_2 = L_3 = L_4 = 10$ cm, $w_1 = w_2 = w_3 = w_4 = 150$ μm, $c_1 = (-450, 0)$ μm, $c_2 = (-150, 0)$ μm, $c_3 = (150, 0)$ μm, $c_4 = (450, 0)$ μm, $N_1 = N_2 = N_3 = N_4 = 9$, $\epsilon_b = 4.7\epsilon_0$, $\sigma_g = 5.92 \times 10^7$ S/m, $h_b = 500$ μm: (a) $v_i = 1$ V, $p(i) = i$, $q(i) = 1$, with $1 \le i \le 4$; (b) $v_1 = 1$ V, $v_2 = -1$ V, $p(1) = 1$, $p(2) = 4$, $q(1) = q(2) = 1$.

investigated. In Fig. 7, we present the field patterns calculated at a distance of 3m at $f = 30$ and 850 MHz, respectively. The metallic coating is made of copper. It is observed that as the frequency increases, the shielding becomes more effective because the electric thickness of the metallic shield increases, especially at higher frequencies.

As the coating thickness increases, the magnitude of E_ϕ on the H plane decreases, and the patterns are roughly the same. The magnitude of E_θ on the E plane reduces significantly around the z direction as the coating thickness is increased. However, the reduction is not as obvious as the angle θ is increased. This can be explained as follows: The current on the trace induces electric current inside the metallic coating. The field generated by the induced current cancels a significant portion of the field generated by the trace in the broadside directions, but the cancellation is less effective around the axial direction of the trace. Similar behaviors are observed with a zinc coating, except that the magnitude of the field is larger than that with the copper coating. This is because the conductivity of zinc is smaller than that of copper.

To summarize the usefulness of the metallic coating, we define the shielding effectiveness (SE) in terms of the maxi-

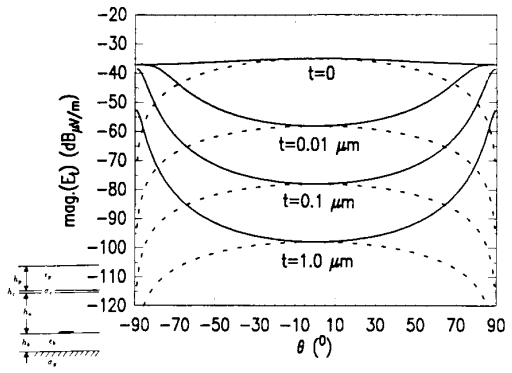

(a)

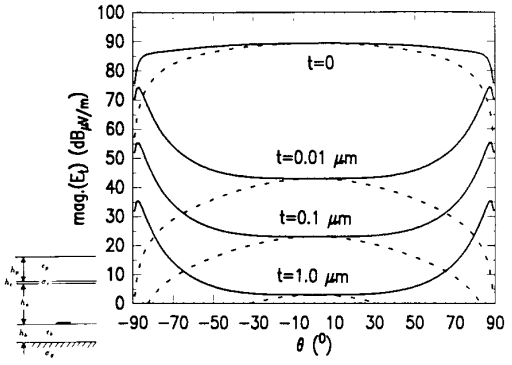

(b)

Fig. 7. Magnitude of tangential electric field from a trace calculated at 3 m, $L_1 = 10$ cm, $w_1 = 150$ μm, $N_1 = 9$, $v_1 = 1$ V, $p(1) = 1$, $q(1) = 1$, $\epsilon_p = 2.7\epsilon_0$, $\epsilon_b = 4.7\epsilon_0$, $\sigma_c = \sigma_g = 5.92 \times 10^7$ S/m, $h_p = 0.5$ cm, $h_c = t$, $h_a = 10$ cm, $h_b = 500$ μm, - - - - E_ϕ at $\phi = 0°$, —— E_θ at $\phi = 90°$: (a) $f = 30$ MHz; (b) $f = 850$ MHz.

mum magnitude of tangential electric fields as

$$\mathrm{SE} = 20 \log_{10} \left| \frac{E_{t,\max}(\text{without shield})}{E_{t,\max}(\text{with shield})} \right|. \qquad (21)$$

The shielding effectiveness in [6] is defined as the ratio of field magnitude at the same location before and after the shield is inserted. Since the plane wave of normal incidence is assumed, there is no need to consider the location of maximum field strength. However, in our cases of interest, the field pattern changes before and after the shield is inserted, and the FCC specification is imposed on the maximum field strength in any possible direction. Hence, it is appropriate to use the definition in (21).

In Fig. 8, we present the shielding effectiveness of metallic coating with three different thicknesses and two different conductivities. It is observed that the shielding effectiveness increases with increasing frequency, conductivity, or physical thickness. In Fig. 9(a) and (b), we present the field patterns of two identical traces driven by two delta gap voltage sources with the same and opposite phase, respectively. It is shown that the effect of the cover alone is very small. In the presence of coating, the maximum field strength occurs around the horizontal directions. Note that with metallic coating, the maximum field strength occurs in the plane of

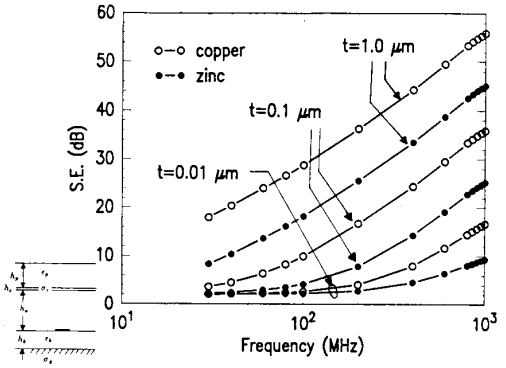

Fig. 8. Shielding effectiveness of metallic coating on radiation from a trace, where $L_1 = 10$ cm, $w_1 = 150$ μm, $N_1 = 9$, $v_1 = 1$ V, $p(1) = 1$, $q(1) = 1$, $\epsilon_p = 2.7\epsilon_0$, $\epsilon_b = 4.7\epsilon_0$, $\sigma_c = 5.92 \times 10^7$, or 1.72×10^7 S/m, $\sigma_g = 5.92 \times 10^7$ S/m, $h_p = 0.5$ cm, $h_c = t$, $h_a = 10$ cm, $h_b = 500$ μm.

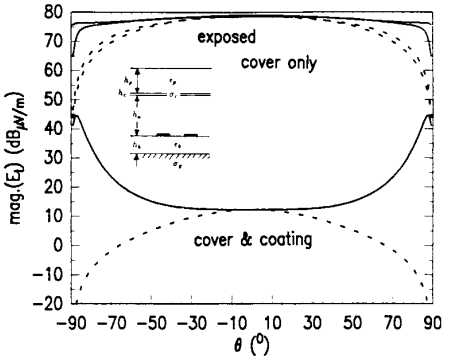

(a)

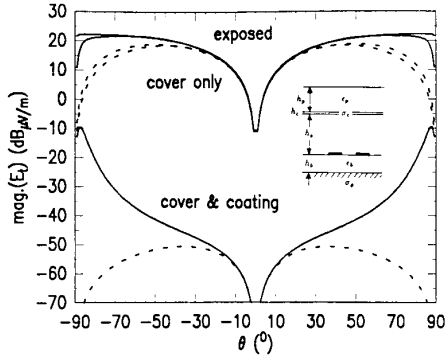

(b)

Fig. 9. Magnitude of tangential electric field from two coupled traces calculated at 3 m, $f = 850$ MHz, $L_1 = L_2 = 10$ cm, $w_1 = w_2 = 150$ μm, $c_1 = (-150, 0)$ μm, $c_2 = (150, 0)$ μm, $N_1 = N_2 = 9$, $p(1) = 1$, $p(2) = 2$, $q(1) = q(2) = 1$, $\epsilon_p = 2.7\epsilon_0$, $\epsilon_b = 4.7\epsilon_0$, $\sigma_c = \sigma_g = 5.92 \times 10^7$ S/m, $h_p = 0.5$ cm, $h_c = 0.1$ μm, $h_a = 10$ cm, $h_b = 500$ μm, —— E_θ, - - - - E_ϕ: (a) $v_1 = 1$ V, $v_2 = 1$ V, $\phi = 0°$; (b) $v_1 = 1$ V, $v_2 = -1$ V, $\phi = 45°$.

$\phi = 0°$ for the common mode and around the plane of $\phi = 45°$ for the differential mode.

The shielding effectiveness with both the even and odd driving source arrangements are shown in Fig. 10. It is found that the shielding effectiveness basically depends on the prop-

erties of the shield and is relatively independent of the driving source arrangements.

VI. Conclusions

A rigorous formulation in the spectral domain is used to investigate the radiation characteristics of coupled unterminated traces in the presence of the plastic cover and coating. The resonant frequencies with different numbers of traces are analyzed. It is found that unterminated traces generate strong radiation around the resonant frequencies. The shielding effectiveness of metallic coating on one and two traces is also analyzed. It is found that the shielding effectiveness mainly depends on the properties of the shield material. Appropriate use of the metallic coating can effectively shield the radiation.

Appendix

For $l = m$ and $z > z'$, the explicit form of $\bar{\bar{g}}_{lm}(\bar{k}_s, z, z')$ is given by [9]–[11]

$$\begin{aligned}\bar{\bar{g}}_{ll}(\bar{k}_s, z_>, z'_<) &= \frac{1}{k_{lz}\left(1 - R^{\mathrm{TE}}_{\cup l} R^{\mathrm{TE}}_{\cap l} e^{2ik_{lz}h_l}\right)} \\ &\quad \left\{\left[\hat{h}(k_{lz}) e^{ik_{lz}z_l} + R^{\mathrm{TE}}_{\cup l}\hat{h}(-k_{lz}) e^{ik_{lz}(2h_l - z_l)}\right]\right. \\ &\quad \left.\left[\hat{h}(k_{lz}) e^{-ik_{lz}z'_l} + R^{\mathrm{TE}}_{\cap l}\hat{h}(-k_{lz}) e^{ik_{lz}z'_l}\right]\right\} \\ &\quad + \frac{l}{k_{lz}\left(l - R^{\mathrm{TM}}_{\cup l} R^{\mathrm{TM}}_{\cap l} e^{2ik_{lz}h_l}\right)} \\ &\quad \left\{\left[\hat{v}(k_{lz}) e^{ik_{lz}z_l} + R^{\mathrm{TM}}_{\cup l}(-k_{lz}) e^{ik_{lz}(2h_l - z_l)}\right]\right. \\ &\quad \left.\left[\hat{v}(k_{lz}) e^{-ik_{lz}z'_l} + R^{\mathrm{TM}}_{\cap l}\hat{v}(-k_{lz}) e^{ik_{lz}z'_l}\right]\right\}. \end{aligned} \tag{A1}$$

For $l = m$ and $z < z'$, we have

$$\begin{aligned}\bar{\bar{g}}_{ll}(\bar{k}_s, z_<, z'_>) &= \frac{1}{k_{lz}\left(1 - R^{\mathrm{TE}}_{\cup l} R^{\mathrm{TE}}_{\cap l} e^{2ik_{lz}h_l}\right)} \\ &\quad \left\{\left[\hat{h}(-k_{lz}) e^{-ik_{lz}z_l} + R^{\mathrm{TE}}_{\cap l}\hat{h}(k_{lz}) e^{ik_{lz}z_l}\right]\right. \\ &\quad \left.\left[\hat{h}(-k_{lz}) e^{ik_{lz}z'_l} + R^{\mathrm{TE}}_{\cup l}\hat{h}(k_{lz}) e^{ik_{lz}(2h_l - z'_l)}\right]\right\} \\ &\quad + \frac{1}{k_{lz}\left(1 - R^{\mathrm{TM}}_{\cup l} R^{\mathrm{TM}}_{\cap l} e^{2ik_{lz}h_l}\right)} \\ &\quad \left\{\left[\hat{v}(-k_{lz}) e^{-ik_{lz}z_l} + R^{\mathrm{TM}}_{\cap l}\hat{v}(k_{lz}) e^{ik_{lz}z_l}\right]\right. \\ &\quad \left.\left[\hat{v}(-k_{lz}) e^{ik_{lz}z'_l} + R^{\mathrm{TM}}_{\cup l}\hat{v}(k_{lz}) e^{ik_{lz}(2h_l - z'_l)}\right]\right\} \end{aligned} \tag{A2}$$

where z_l and z'_l are the local coordinates defined as $z_l = z + d_l$, $z'_l = z' + d_l$, and

$$\hat{h}(\pm k_{lz}) = \frac{\hat{x}k_y - \hat{y}k_x}{k_s}$$

$$\hat{v}(\pm k_{lz}) = \mp \frac{k_{lz}\bar{k}_s}{k_l k_s} + \hat{z}\frac{k_s}{k_l} \tag{A3}$$

where $k_s = |\bar{k}_s|$, $k_{lz} = \sqrt{k_l^2 - k_s^2}$ with $\mathrm{Im}(k_{lz}) \geq 0$.

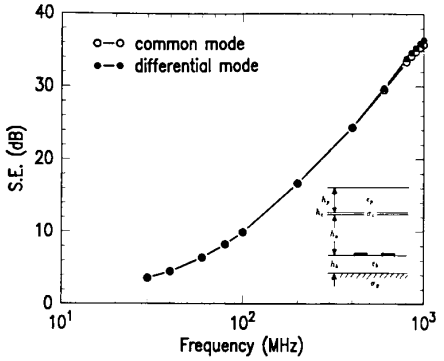

Fig. 10. Shielding effectiveness of metallic coating on radiation from two coupled traces, where $L_1 = L_2 = 10$ cm, $w_1 = w_2 = 150$ μm, $c_1 = (-150, 0)$ μm, $c_2 = (150, 0)$ μm, $N_1 = N_2 = 9$, $v_1 = 1$ V, $v_2 = \pm 1$ V, $p(1) = 1$, $p(2) = 2$, $q(1) = q(2) = 1$, $\epsilon_p = 2.7\epsilon_0$, $\epsilon_b = 4.7\epsilon_0$, $\sigma_c = \sigma_g = 5.92 \times 10^7$ S/m, $h_p = 0.5$ cm, $h_c = 0.1$ μm, $h_a = 10$ cm, $h_b = 500$ μm.

In (A1) and (A2), $R^{\mathrm{TM}}_{\cup m}$ and $R^{\mathrm{TE}}_{\cup m}$ are the reflection coefficients of the TM and TE modes at the upper boundary of layer (m), $R^{\mathrm{TM}}_{\cap m}$ and $R^{\mathrm{TE}}_{\cap m}$ are the reflection coefficients of the TM and TE modes at the lower boundary of layer (m). They can be obtained recursively as

$$R^{\alpha}_{\cup m} = \frac{R^{\alpha}_{m(m-1)} + R^{\alpha}_{\cup(m-1)} e^{2ik_{(m-1)z}h_{m-1}}}{1 + R^{\alpha}_{m(m-1)} R^{\alpha}_{\cup(m-1)} e^{2ik_{(m-1)z}h_{m-1}}},$$

$$\alpha = (\mathrm{TM}, \mathrm{TE})$$

$$R^{\alpha}_{\cap m} = \frac{R^{\alpha}_{m(m+1)} + R^{\alpha}_{\cap(m+1)} e^{2ik_{(m+1)z}h_{m+1}}}{1 + R^{\alpha}_{m(m+1)} R^{\alpha}_{\cap(m+1)} e^{2ik_{(m+1)z}h_{m+1}}},$$

$$\alpha = (\mathrm{TM}, \mathrm{TE}) \tag{A4}$$

where $R^{\alpha}_{m(m-1)}$ and $R^{\alpha}_{m(m+1)}$ are the Fresnel reflection coefficients of the α mode across the interfaces at $z = -d_{m-1}$ and $z = -d_m$, respectively. The explicit forms are

$$R^{\mathrm{TM}}_{m(m\pm1)} = \frac{\epsilon_{m\pm1}k_{mz} - \epsilon_m k_{(m\pm1)z}}{\epsilon_{m\pm1}k_{mz} + \epsilon_m k_{(m\pm1)z}},$$

$$R^{\mathrm{TE}}_{m(m\pm1)} = \frac{k_{mz} - k_{(m\pm1)z}}{k_{mz} + k_{(m\pm1)z}}. \tag{A5}$$

For the case of $l < m$, we have

$$\begin{aligned}\bar{\bar{g}}_{lm}(\bar{k}_s, z_>, z'_<) &= \frac{X^{\mathrm{TE}}_{\cup l}}{k_{mz}\left(1 - R^{\mathrm{TE}}_{\cup m} R^{\mathrm{TE}}_{\cap m} e^{2ik_{mz}h_m}\right)} \\ &\quad \left\{\left[\hat{h}(k_{lz}) e^{ik_{lz}z_l} + R^{\mathrm{TE}}_{\cup l}\hat{h}(-k_{lz}) e^{ik_{lz}(2h_l - z_l)}\right]\right. \\ &\quad \left.\left[\hat{h}(k_{mz}) e^{-ik_{mz}z'_m} + R^{\mathrm{TE}}_{\cap m}\hat{h}(-k_{mz}) e^{ik_{mz}(2h_m + z'_m)}\right]\right\} \\ &\quad + \frac{X^{\mathrm{TM}}_{\cup l}}{k_{mz}\left(1 - R^{\mathrm{TM}}_{\cup m} R^{\mathrm{TM}}_{\cap m} e^{2ik_{mz}h_m}\right)} \\ &\quad \left\{\left[\hat{v}(k_{lz}) e^{ik_{lz}z_l} + R^{\mathrm{TM}}_{\cup l}\hat{v}(-k_{lz}) e^{ik_{lz}(2h_l - z_l)}\right]\right. \\ &\quad \left.\left[\hat{v}(k_{mz}) e^{-ik_{mz}z'_m} + R^{\mathrm{TM}}_{\cap m}\hat{v}(-k_{mz}) e^{ik_{mz}(2h_m + z'_m)}\right]\right\} \end{aligned} \tag{A6}$$

where z_l and z'_m are the local coordinates defined as $z_l = z + d_l$ and $z'_m = z' + d_{m-1}$, respectively; $\hat{h}(\pm k_{bz})$ and $\hat{v}(\pm k_{bz})$ with $b = l, m$ are defined in (A3).

For the case of $l > m$, we have

$$\begin{aligned}\bar{\bar{g}}_{lm}(\bar{k}_s, z_<, z'_>) &= \frac{X^{\mathrm{TE}}_{\cap l}}{k_{mz}\left(1 - R^{\mathrm{TE}}_{\cup m} R^{\mathrm{TE}}_{\cap m} e^{2ik_{mz}h_m}\right)} \\ &\quad \left\{\left[\hat{h}(-k_{lz})e^{-k_{lz}z_l} + R^{\mathrm{TE}}_{\cap l}\hat{h}(k_{lz})e^{ik_{lz}(2h_l + z_l)}\right]\right. \\ &\quad \left.\left[\hat{h}(-k_{mz})e^{ik_{mz}z'_m} + R^{\mathrm{TE}}_{\cup m}\hat{h}(k_{mz})e^{ik_{mz}(2h_m - z'_m)}\right]\right\} \\ &\quad + \frac{X^{\mathrm{TM}}_{\cap l}}{k_{mz}\left(1 - R^{\mathrm{TM}}_{\cup m} R^{\mathrm{TM}}_{\cap m} e^{2ik_{mz}h_m}\right)} \\ &\quad \left\{\left[\hat{v}(-k_{lz})e^{-ik_{lz}z_l} + R^{\mathrm{TM}}_{\cap l}\hat{v}(k_{lz})e^{ik_{lz}(2h_l + z_l)}\right]\right. \\ &\quad \left.\left[\hat{v}(-k_{mz})e^{ik_{mz}z'_m} + R^{\mathrm{TM}}_{\cup m}\hat{v}(k_{mz})e^{ik_{mz}(2h_m - z'_m)}\right]\right\} \end{aligned} \tag{A7}$$

where z_l and z'_m are the local coordinates defined as $z_l = z + d_{l-1}$ and $z'_m = z' + d_m$, respectively. In (A6) and (A7), $X^{\alpha}_{\cup l}$ is the upward transmission coefficient of the α mode, and $X^{\alpha}_{\cap l}$ is the downward transmission coefficient of the α mode, where $\alpha = \mathrm{TE}, \mathrm{TM}$. These coefficients can be calculated recursively by

$$X^{\alpha}_{\cup l} = X^{\alpha}_{\cup(l+1)} e^{ik(l+1)z^{h_l + l}} p^{\alpha}_{l(l+1)} \frac{1 + s_\alpha R^{\alpha}_{\cup(l+1)}}{1 + s_\alpha R^{\alpha}_{\cup l} e^{2ik_{lz}h_l}},$$

$$l = m - 2, m - 3, \cdots, 0$$

$$X^{\alpha}_{\cup(m-1)} = p^{\alpha}_{(m-1)m} \frac{1 + s_\alpha R^{\alpha}_{\cup m}}{1 + s_\alpha R^{\alpha}_{\cup(m-1)} e^{2ik(m-1)z^{h_{m-1}}}},$$

$$l = m - 1$$

$$X^{\alpha}_{\cap l} = X^{\alpha}_{\cap(l-1)} e^{ik(l-1)z^{h_{l-1}}} p^{\alpha}_{l(l-1)} \frac{1 - s_\alpha R^{\alpha}_{\cap(l-1)}}{1 + s_\alpha R^{\alpha}_{\cap l} e^{2ik_{lz}h_l}},$$

$$l = m + 2, m + 3, \cdots, n$$

$$X^{\alpha}_{\cap(m+1)} = p^{\alpha}_{(m+1)m} \frac{1 + s_\alpha R^{\alpha}_{\cap m}}{1 + s_\alpha R^{\alpha}_{\cap(m+1)} e^{2ik(m+1)z^{h_m + 1}}},$$

$$l = m + 1 \tag{A8}$$

where

$$s_\alpha = \begin{cases} 1, & \alpha = \mathrm{TE} \\ -1, & \alpha = \mathrm{TM} \end{cases} \tag{A9}$$

and

$$p^{\alpha}_{ij} = \begin{cases} 1, & \alpha = \mathrm{TE} \\ (k_i k_{jz})/(k_j k_{iz}), & \alpha = \mathrm{TM}. \end{cases} \tag{A10}$$

Acknowledgment

The author would like to thank D. J. McBride, B. J. Rubin, S. Daijavad, and the anonymous reviewers for their useful comments.

References

[1] B. Keiser, *Principles of Electromagnetic Compatibility* (3rd ed.). Norwood, MA: Artech House, 1987, ch. 20.

[2] I. J. Bahl and P. Bhartia, *Microstrip Antennas*. Dedham, MA: Artech House, 1980.

[3] K. R. Carver and J. W. Mink, "Microstrip antenna technology," *IEEE Trans. Antennas Propagat.*, vol. AP-29, no. 1, pp. 2-24, Jan. 1981.

[4] I. E. Rana and N. G. Alexopoulos, "Current distribution and input impedance of printed dipoles," *IEEE Trans. Antennas Propagat.*, vol. AP-29, no. 1, pp. 99-105, Jan. 1981.

[5] D. M. Pozar, "Considerations for millimeter wave printed antennas," *IEEE Trans. Antennas Propagat.*, vol. AP-31, no. 5, pp. 740-747, Sept. 1983.

[6] S. Y. Liao, "RF shielding effectiveness and light transmission of copper or silver film coating on plastic substrate," *IEEE Trans. Electromagn. Compat.*, vol. EMC-18, no. 4, pp. 148-153, Nov. 1976.

[7] R. B. Schulz, V. C. Plantz, and D. R. Brush, "Shielding theory and practice," *IEEE Trans. Electromagn. Compat.*, vol. 30, no. 3, pp. 187-201, Aug. 1988.

[8] B. J. Rubin, "The propagation characteristics of signal lines in a mesh-plane environment," *IEEE Trans. Microwave Theory Tech.*, vol. MTT-32, no. 5, pp. 522-531, May 1984.

[9] J. F. Kiang, S. M. Ali, and J. A. Kong, "Propagation properties of striplines periodically loaded with crossing strips," *IEEE Trans. Microwave Theory Tech.*, vol. 37, no. 4, pp. 776-786, Apr. 1989.

[10] J. A. Kong, *Electromagnetic Waves Theory*. New York: Wiley, 1986.

[11] S. M. Ali, T. M. Habashy, and J. A. Kong, "Dyadic Green's function for anisotropic multilayered media," *J. Electromag. Waves Appl.*, to be published.

[12] C. R. Paul, "A comparison of the contributions of common-mode and differential-mode currents in radiated emissions," *IEEE Trans. Electromagn. Compat.*, vol. 31, no. 2, pp. 189-193, May 1989.